Int. J. Electrochem. Sci., 6 **(2011)** 3210 - 3223

International Journal of
ELECTROCHEMICAL
SCIENCE
www.electrochemsci.org

Synthesis and Characterization of Long Life $Li_4Ti_5O_{12}$/C Composite Using Amorphous TiO_2 Nanoparticles

Baohua Li[1], *Feng Ning*[1], *Yan-Bing He*[1,*], *Hongda Du*[1], *Quan-Hong Yang*[1], *Jun Ma*[1], *Feiyu Kang*[1, 2*], *Chin-Tsau Hsu*[1]

[1] Key Laboratory of Thermal Management Engineering and Materials, Graduate School at Shenzhen, Tsinghua University, Shenzhen, 518055, China
[2] Laboratory of Advanced Materials, Department of Materials Science and Engineering, Tsinghua University, Beijing, 100084, China
[*]E-mail: hezuzhang_2000@163.com, fykang@mail.tsinghua.edu.cn

Received: 12 June 2011 / *Accepted:* 29 June 2011 / *Published:* 1 August 2011

Amorphous TiO_2 nanoparticles are synthesized by microemulsion method using cetyltrimethylammonium bromide (CTAB) as dispersant for the first time, and then they are used to synthesize the $Li_4Ti_5O_{12}$/C composite by a simple solid-state method. The amorphous TiO_2 nanoparticles have high reaction activity with Li_2CO_3 to promote the synthesis of $Li_4Ti_5O_{12}$/C composite at lower temperature and shorter time. The grain size of prepared $Li_4Ti_5O_{12}$/C composite with different carbon additions is less than 400 nm. The $Li_4Ti_5O_{12}$/C composite shows high specific capacity and very long cycling life. The specific capacities of the $Li_4Ti_5O_{12}$/C composite with 5% carbon addition at 0.1, 1 and 5 C rates are 162.4, 147.4 and 114.9 $mAhg^{-1}$, respectively, and its capacity retention after 600 cycles at 1 and 5 C rates is respective 99.86% and 92.95%. The synthesis method can be used for a mass production of $Li_4Ti_5O_{12}$/C composite in industry.

Keywords: Amorphous TiO_2 nanoparticles, $Li_4Ti_5O_{12}$/C composite, solid-state method, electrochemical performance

1. INTRODUCTION

Spinel $Li_4Ti_5O_{12}$ material has an excellent reversibility of Li-ion intercalation and de-intercalation with a theoretical capacity of $175mAhg^{-1}$, and also exhibits zero strain volume change during charge and discharge cycles with an excellent safety performance [1-3]. It also has a very flat voltage plateau at around 1.55V (vs. Li/Li^+), which is higher than the reduction potential of most organic electrolytes [4-6]. Being much safer and more stable than carbon-based materials, $Li_4Ti_5O_{12}$ has been demonstrated as a good candidate of negative electrode material for long-life lithium-ion

power batteries. However, the power performance of $Li_4Ti_5O_{12}$ is greatly limited by its low electronic conductivity. In order to improve the electrochemical performance of $Li_4Ti_5O_{12}$, extensive works had been concentrated on forming nanoparticles [7-10], doping [11-16] with metal cations and composing with carbon or metal powder [14,17-22]. The formation of nanoparticles can reduce the Li-ion diffusion path, as well as provide large contact area between the nanoparticles. Doping by other metal cations and adding carbon or metal powder into the $Li_4Ti_5O_{12}$ can increase the electronic conductivity to improve the electrochemical performance greatly.

Even though nano-sized $Li_4Ti_5O_{12}$ particles had been successfully prepared using advanced techniques such as sol-gel process [3,17,23-24], the solid-state reaction remains as the most attractive process for potential industrial application because of the abundance of TiO_2 as titanium source at low cost [11-15,25-26]. In spite of suffering from high calcination temperature, large grain size, impurity phases and lithium evaporation, the solid-state method has obvious advantages of simple synthesis, facile scale up and well-crystallized products. The solid-state method usually uses the TiO_2 and Li_2CO_3/LiOH as the raw materials. Anatase TiO_2 is generally considered to be the most active Li-ion insertion host, and has been used in most studies as the starting material for synthesizing $Li_4Ti_5O_{12}$ [8,25,27-29]. However, it is difficult to synthesize the nano-sized $Li_4Ti_5O_{12}$ using anatase TiO_2 by solid-state method.

It is well-known that the amorphous TiO_2 has larger surface area, which also can react with the Li_2CO_3/LiOH to form $Li_4Ti_5O_{12}$. Yang et al. [30] reported that the $Li_4Ti_5O_{12}$ with particles size of 2.66μm can be synthesized using the amorphous TiO_2 (grain size≤1μ) and Li_2CO_3 at 950 ^oC for 24h. We also found another report using the amorphous TiO_2 and LiOH to prepare the $Li_4Ti_5O_{12}$ at 800 ^oC for 16h [31]. Whereas, above $Li_4Ti_5O_{12}$ materials all showed bad cycling and rate discharge performance, especially the high rate cycling performance. In this paper, we adapted the microemulsion method to synthesize the amorphous TiO_2 nanoparticles for the first time, which was then used to synthesize the $Li_4Ti_5O_{12}$/C composite with solid-state method. We find that the amorphous TiO_2 nanoparticles as prepared using microemulsion method have high reaction activity with Li_2CO_3 to promote the synthesis of $Li_4Ti_5O_{12}$/C at lower temperature and shorter time. The $Li_4Ti_5O_{12}$/C composite with particle size less than 400 nm was synthesized successfully using as prepared amorphous TiO_2 nanoparticles at 800 ^oC for 12h, which shows high specific capacity and excellent cycling stability. This method has a potential for a mass production of $Li_4Ti_5O_{12}$/C composite in industry.

2. EXPERIMENTAL

2.1 Preparation of amorphous TiO_2 nanoparticles

The saturated solution of cetyltrimethylammonium bromide (CTAB) was prepared with the deionized water under continuous stirring for 2h. The butyl titanate ($Ti(OC_4H_9)_4$) was then added into the CTAB solution under ultrasound mixing. Then the stoichiometric ammonia was added under

ultrasound mixing for 15min and continuous stirring for 2h. The resultant solution of amorphous TiO_2 was filtrated and dried to obtain the amorphous TiO_2 nanoparticles.

2.2 Preparation of $Li_4Ti_5O_{12}$/C composite

$Li_4Ti_5O_{12}$ was synthesized by solid-state method using the amorphous TiO_2 nanoparticles prepared above and the Li_2CO_3 obtained commercially. The precursors of amorphous TiO_2 nanoparticles and Li_2CO_3 were mixed at the Li:Ti molar ratio of 4.2:5. The precursors were ground for 6 h by a wet ball-milling in an acetone solution. The resultant stable gel was dried at 80 °C to form a mixed dry precursor. The dried powder precursor was then calcinated at 800 ^oC for 12 h in argon atmosphere to obtain $Li_4Ti_5O_{12}$. The $Li_4Ti_5O_{12}$/C composite with different carbon contents was also prepared by using a similar solid-state method mentioned above. In this case, however, it was prepared from a ternary precursor mixture of the amorphous TiO_2, Li_2CO_3 and glucose. The thermogravimetric (TG) measurements for precursors of the amorphous TiO_2 and Li_2CO_3 at air and argon atmosphere were conducted with a heating rate of 10 $^oCmin^{-1}$ from room temperature to 800 ^oC by using a Rigaku Thermo Plus TG8120 system.

2.3 Structure and morphology characterization of prepared powders

X-ray diffraction (XRD) patterns of the samples were obtained by a Rigaku D/max 2500/PC diffractometer using Cu Kα radiation in an angular range of 10-90^o (2θ) with a 0.02^o (2θ) step. The microstructure and morphology of the prepared powders was observed with an environment scanning electron microscope (FE-SEM, HITACH S4800) and transmission electron microscopy (TEM, JOEL JSM-2100F). The specific surface areas of samples were measured using the multi-point (8) Brunauer-Emmett-Teller (BET) technique (Micromeritics ASAP 2020).

2.4 Cell assembly and testing

2032-type coin cells were manufactured to study the electrochemical performance of $Li_4Ti_5O_{12}$/C composite. The coin cells used the $Li_4Ti_5O_{12}$/C composite as cathode material, lithium foil as anode, and polypropylene as separator. The cathode consisted of 80 wt% $Li_4Ti_5O_{12}$/C composite, 10 wt% Super-P and 10 wt% poly(vinylidene fluoride) (PVDF). The electrolyte was 1 M $LiPF_6$ in a 1:1 mixture of ethylene carbonate and diethyl carbonate (1 M $LiPF_6$/ EC+DEC). The cells were assembled in a glove box filled with high purity argon gas.

The electrochemical workstation (VMP3) was used to measure the cyclic voltammograms (CV) and the electrochemical impedance spectrum (EIS) of cells. EIS of the coin cells were measured at half state of charge using $Li_4Ti_5O_{12}$/C as the working electrode and lithium as both the reference and counter electrodes. The impedance was measured by applying a 5 mV ac oscillation with the frequency ranging from 100 kHz to 0.01 Hz. The CV of coin cells were measured with $Li_4Ti_5O_{12}$/C electrode as the working electrode, lithium foil as both the reference and counter electrodes. A scanning rate of

$0.1mVs^{-1}$ was applied with a sweep voltage range of 2.5~0.5 V (vs. Li/Li^+). The cycling and rate discharge performance were characterized by using a Land 2001A cell test system (Wuhan, China) at room temperature.

3. RESULTS AND DISCUSION

3.1 Structure and morphology of amorphous TiO_2 nanoparticles

The amorphous TiO_2 was synthesized using microemulsion method in which the surfactant, cetyltrimethylammonium bromide (CTAB), was used as dispersant. Fig.1 shows the XRD patterns and SEM images of as-prepared TiO_2. From Fig. 1a, it is found that the XRD patterns do not contain the peaks corresponding to the anatase and rutile phases. Thus, the as-prepared TiO_2 is predominantly in amorphous phase. As shown in Fig. 1b and 1c, the amorphous TiO_2 consists of spherical particles with average diameter of 200-300 nm, which are the agglomerates of much smaller primary particles with diameter of about 10-20 nm. The amorphous TiO_2 nanoparticles show highly ordered structure with well-defined secondary and primary particles. The smaller primary particles help to improve the reaction activity of amorphous TiO_2 with Li_2CO_3.

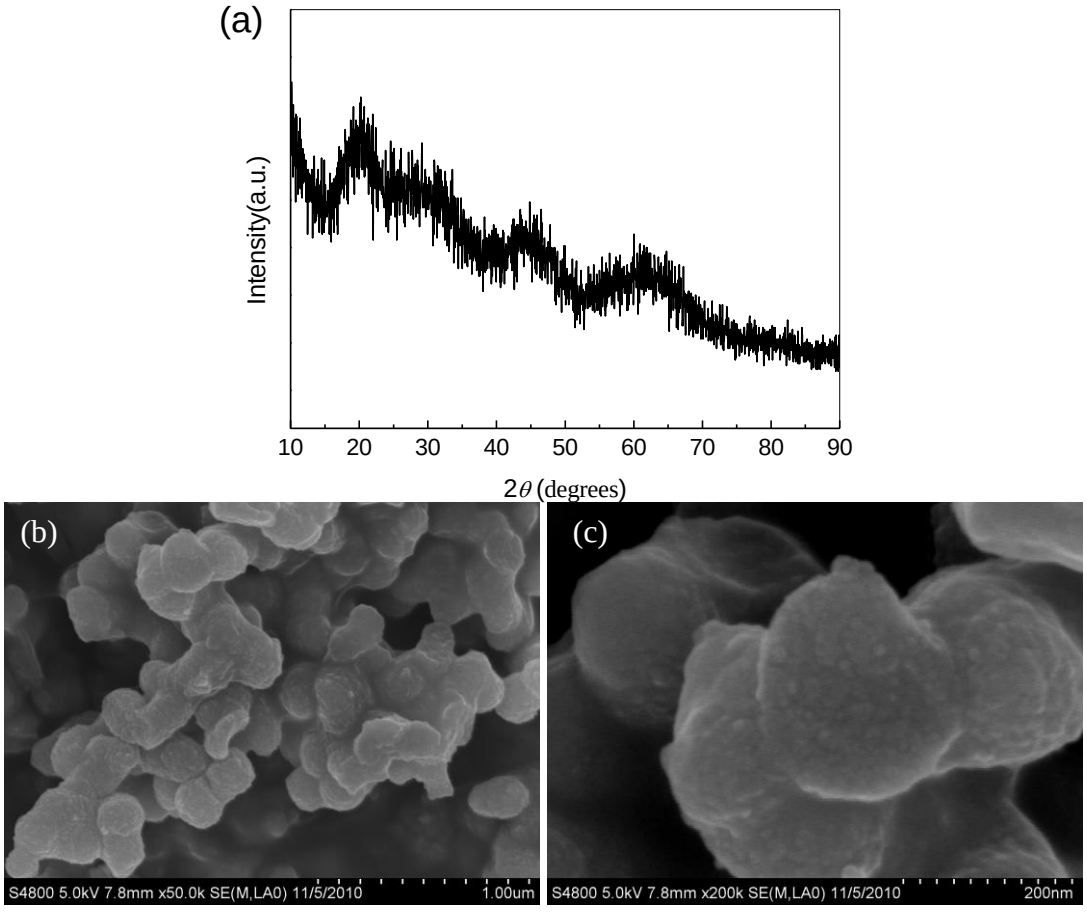

Figure 1. XRD patterns (a) and SEM images of as-prepared TiO_2 at 20k×(b) and 50k×(c).

3.2 TG analysis of amorphous TiO_2 and Li_2CO_3

Fig. 2 shows the TG curves of precursors of amorphous TiO_2 and Li_2CO_3 in air and argon atmospheres. It is seen that the weight loss of the precursors in air is 40.54 wt% and that in argon is 38.87 wt% from 60 to 800 ^oC. Thus, the amount of residual carbon in the $Li_4Ti_5O_{12}$ material in argon is about 1.67 wt%. The weight loss of precursors in air atmosphere is mainly due to the quickly dehydration of amorphous TiO_2 and decomposition of Li_2CO_3. In addition, the filtration products of amorphous TiO_2 could not be washed completed with the deionized water, i.e., some CTAB still existed in the amorphous TiO_2 nanoparticles. Thus, the CTAB also was decomposed to the residual carbon at argon and the residual carbon was further combusted in air at about 500 ^oC. It is also found from the TG curves that the weight remains constant above 500 ^oC in argon and 550 ^oC in air, which indicates that the Li_2CO_3 has been decomposed. As it is well-known that the decomposition temperature of Li_2CO_3 is above 700 ^oC, and the low reaction temperature between amorphous TiO_2 and Li_2CO_3 ($\leq$500 ^oC) suggests that the amorphous TiO_2 has high reaction activity with Li_2CO_3 to promote the synthesis of $Li_4Ti_5O_{12}$/C at lower temperature. The formation temperature of $Li_4Ti_5O_{12}$ using amorphous TiO_2 and Li_2CO_3 is obviously lower than others reported [14,30,32]. We also tested the actual carbon content of $Li_4Ti_5O_{12}$/C composite with 3 and 5 wt% carbon additions using glucose by calcination at air atmosphere, it was found that the actual carbon content is higher, of about 4.5 and 6.3 wt%, due to the decomposition of CTAB in addition to that of glucose.

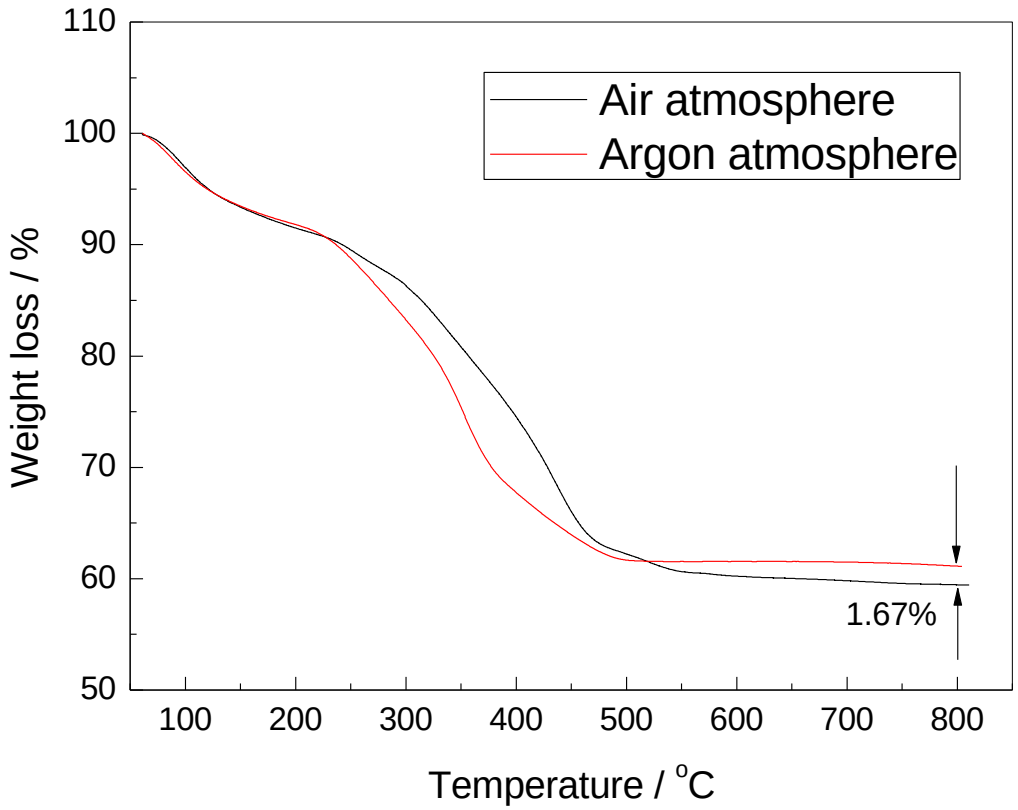

Figure 2. TG curves of precursors of amorphous TiO_2 and Li_2CO_3 in air and argon environments.

3.4 Phase analysis of $Li_4Ti_5O_{12}$/C composite

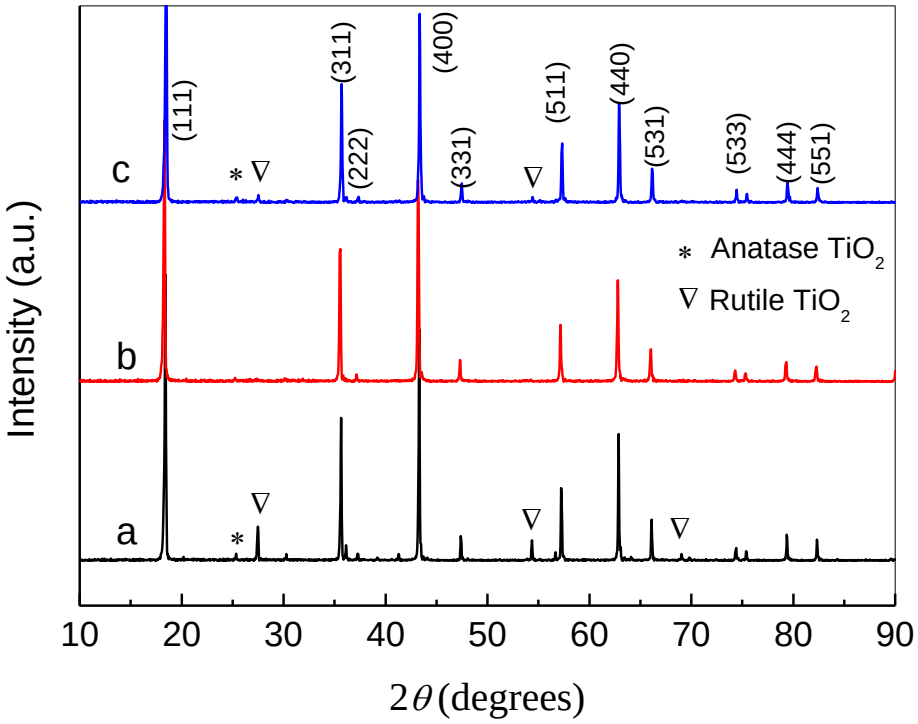

Figure 3. XRD patterns of $Li_4Ti_5O_{12}$/C composite with different carbon additions using glucose: (a) 0 wt%, (b) 3 wt%, and (c) 5 wt%.

The XRD patterns of $Li_4Ti_5O_{12}$/C composites with different carbon additions are shown in Fig. 3. It is seen that the crystal structure of the samples is greatly changed with carbon addition. The XRD patterns of $Li_4Ti_5O_{12}$ without the glucose addition shows obviously the impurity phase peaks of rutile and anatase TiO_2, but not the phase peaks of carbon. Thus, the carbon is in amorphous state. When 3 wt% carbon is added into the precursors of amorphous TiO_2 and Li_2CO_3, no impurity phase peaks can be identified in the $Li_4Ti_5O_{12}$/C composite.

The XRD pattern is in good agreement with JCPDS file (card No. 26-1198), confirming the formation of pure $Li_4Ti_5O_{12}$. The diffraction peaks can be indexed on the spinel structure of $Li_4Ti_5O_{12}$ with the space group *Fd*3*m*. No diffraction response of carbon in XRD patterns is observed due to low content and amorphous state of carbon. When 5 wt% carbon is added into the precursors of amorphous TiO_2 and Li_2CO_3, the XRD patterns of $Li_4Ti_5O_{12}$/C composite contain again the slight impurity phase peaks of rutile and anatase TiO_2. Therefore, it can be concluded that the amount of glucose in the precursors of amorphous TiO_2 and Li_2CO_3 affects the syntheses of $Li_4Ti_5O_{12}$/C composite materials greatly. The carbon addition plays an important role in controlling the impurity phases of anatase and rutile TiO_2.

It is well-known that the formation of the impurity phases of rutile and anatase TiO_2 is mainly attributed to the lithium evaporation. The added glucose is at first uniformly distributed in the matrix of amorphous TiO_2 and Li_2CO_3, which can reduce the lithium evaporation at high temperature.

However, too much carbon will hinder the reaction of amorphous TiO_2 and Li_2CO_3, and also lead to some lithium evaporation, which results in the formation of the impurity phases of rutile and anatase TiO_2.

3.5 Morphology of $Li_4Ti_5O_{12}$/C composite

The SEM and TEM images of the as-prepared $Li_4Ti_5O_{12}$/C with different carbon contents as shown in Fig. 4 were obtained to characterize the effect of the carbon addition on the morphology of $Li_4Ti_5O_{12}$/C composite. It is seen that the grain size of as prepared $Li_4Ti_5O_{12}$/C composite with different carbon addition is less than 400 nm.

Fig. 4a presents that some small particles and free amorphous materials exist in the sample. From the XRD patterns as shown in Fig. 3a, it can be found that the free amorphous materials may be the carbon and the small particles may be the anatase TiO_2. The $Li_4Ti_5O_{12}$ particles are relatively smooth and show the characteristics of spinel structure. From the high resolution TEM image (Fig. 4b), it can be identified that the $Li_4Ti_5O_{12}$ particles are coated with thin-layers of thickness of 0.5 nm, which may be the carbon thin film. The carbon nano-layers and free carbon are attributed to the decomposition of CTAB at high temperature.

Whereas, the samples with 3 wt% carbon addition almost neither contain small particles nor amorphous materials (see Fig. 4c). Combining with the XRD patterns shown in Fig. 3, it can be inferred that the samples neither contain the amorphous carbon nor the anatase TiO_2. It is also interesting to note that the $Li_4Ti_5O_{12}$ particles are covered by relatively thick surface layers and almost does not show the characteristics of the spinel structure from the morphology of samples.

The TEM image shown in Fig. 4d indicates that several carbon layers of thickness of 2-5 nm with interlayer spacing of around 0.5 nm are uniformly coated on the well-crystallized $Li_4Ti_5O_{12}$ particles. The layered carbon images are obvious different from those reported by others [17-18]. The multilayer carbon is attributed to the decomposition of CTAB and glucose. With the increase of carbon addition, it can be seen also from the image of Fig. 4e that the samples with 5 wt% carbon addition contain some free amorphous carbon materials, which indicates that too much carbon addition may lead to the agglomeration of carbon.

The TEM image of Fig. 4f also shows that the surface of large $Li_4Ti_5O_{12}$ particles is covered by irregular carbon particles to exhibit a rougher surface. The amorphous carbon is formed because the temperature of heat-treatment is below 1000^oC. During the heat-treatment, fine $Li_4Ti_5O_{12}$ particles aggregate together to become larger particles. Meanwhile, the CTAB and added glucose turn into carbon, with one part of carbon given away to produce carbon oxides to hinder the agglomeration process. The remaining carbons move to the surface of the fine $Li_4Ti_5O_{12}$particles and appear as a nano coating layer [8,18]. Of course, too much remaining carbon would lead to the agglomeration of carbon as shown in Fig. 4e.

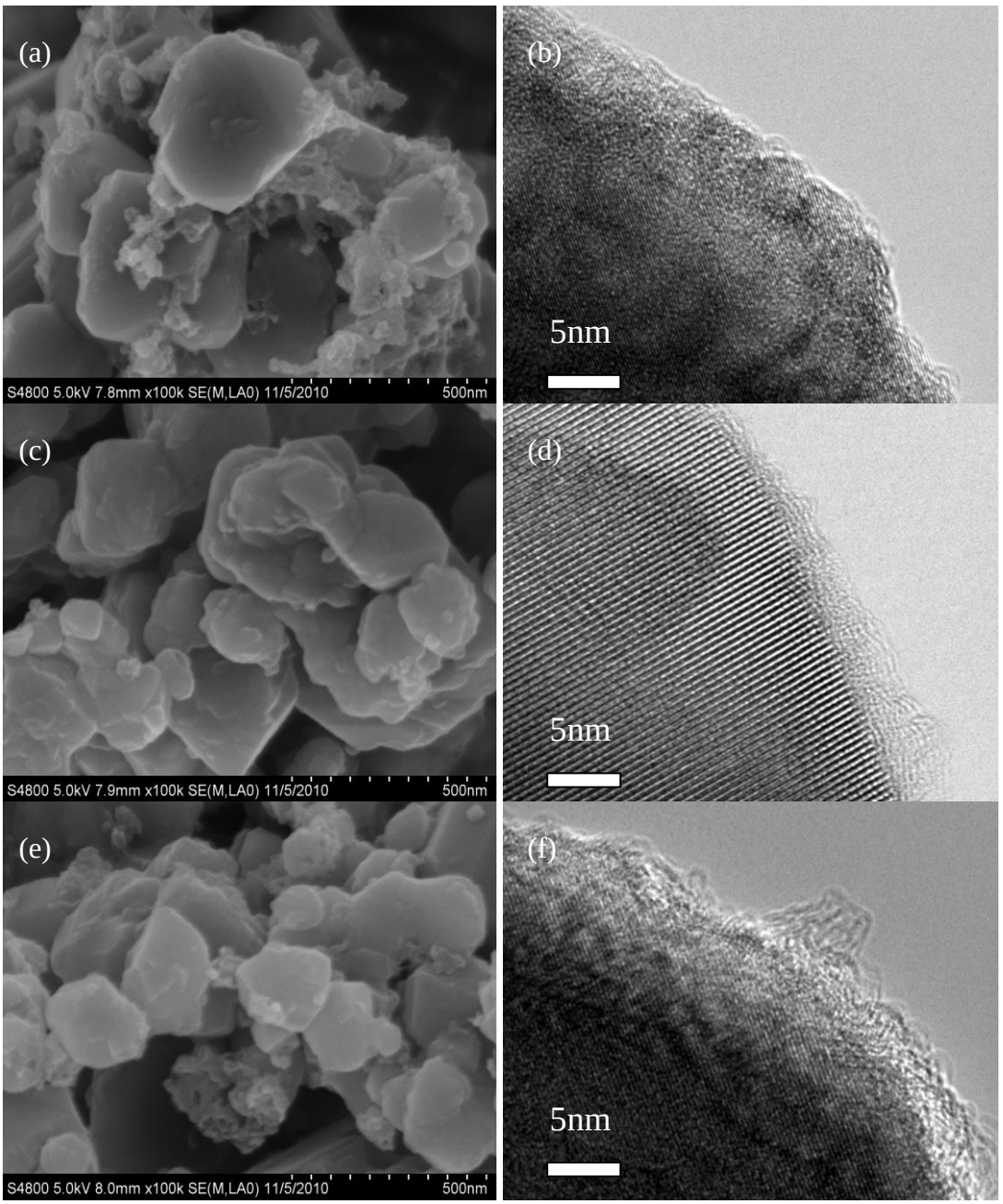

Figure 4. SEM and TEM images of $Li_4Ti_5O_{12}$/C composite with different carbon additions using glucose: 0 wt % (a) and (b), 3 wt% (c) and (d), and 5 wt% (e) and (f).

Table 1 shows the BET surface areas of the $Li_4Ti_5O_{12}$ with different carbon additions. The BET surface areas of samples with 0, 3 and 5 wt% carbon addition are 19.6, 13.4 and 28.4 m^2g^{-1}. The sample with 3 wt% carbon addition has the least BET surface area, which increases greatly as carbon addition increases to 5 wt%. This result indicates that the sample with 3 wt% carbon addition contains almost no free amorphous carbon, which is consistent with the image shown in Fig. 4. The existence of free amorphous carbon as shown in Figs. 4a and 4e results in an obvious increase in the surface area of $Li_4Ti_5O_{12}$/C composite.

Table 1. BET surface areas of the $Li_4Ti_5O_{12}$/C composite with different carbon additions

Carbon addition (wt%)	0	3	5
Surface areas (m^2g^{-1})	19.6	13.4	28.4

3.6 CV and EIS characterization of $Li_4Ti_5O_{12}$/C composite

It has been shown in Figs. 3 and 4 that the microstructure and morphology of $Li_4Ti_5O_{12}$ samples change greatly with the increase of carbon addition. Here we investigate the electrochemical performance of $Li_4Ti_5O_{12}$ samples with different carbon additions. Figs. 5a and 5b show respectively the CV and EIS of $Li_4Ti_5O_{12}$ with 0, 3 and 5 wt% carbon additions. It can be seen from Fig. 5a that the cathodic peaks occur at 1.71, 1.67 and 1.70 V for the $Li_4Ti_5O_{12}$ sample with 0, 3 and 5 wt% carbon additions, respectively, while the corresponding anodic peaks are 1.42, 1.45 and 1.41 V. Note that the sample with 3 wt% carbon addition has higher lithiation potential and lower delithiation potential than those of other samples. In addition, the lithiation and delithiation peak currents of $Li_4Ti_5O_{12}$ sample with 3 wt% carbon addition are obviously greater than other samples, with the sample with 5 wt% carbon addition showing the least peak current, whereas it is seen that the sample with 5 wt% carbon addition shows obviously characteristic of double-layer and redox capacitance due to the high BET surface areas. Thus, it can be concluded that the $Li_4Ti_5O_{12}$ sample with 3 wt% carbon addition have the least electrochemical reaction polarization. The polarization increases as the carbon content increases or decreases.

We have known from Fig. 3 that only the sample with 3 wt% carbon addition does not show the agglomeration of carbon, but not the samples with 0 and 5wt% carbon additions. Since higher electronic and ionic conductivities imply higher the electrochemical reaction rate, it is easily understandable that, the more the agglomerration occurs with increasing carbon fraction, the larger is the tortuosity of voids that decreases greatly the ionic conducition through the pore space of the electrodes [18]. Although the agglomerration can improve the electronic conductivity of active material to some extent, the much lower ionic conducitvity increases the polarization greatly. Therefore, the lithiation/delithiation of $Li_4Ti_5O_{12}$ samples become difficult with the increase of carbon fraction. It is observed that the oxidation and reduction peaks of sample with 5 wt% carbon addition is lower and wider, indicating that the charge storage mechanism may include the lithium ion lithiation and capacitive behavior due to the BET surface areas. When the amorphous carbon fraction increases, considerably large charge of the double-layer and side interface reactions on $Li_4Ti_5O_{12}$ sample surface may occur.

The EIS results of $Li_4Ti_5O_{12}$/Li half cells after five cycles are plotted in Fig. 5b. All cells were cycled 3 times before the EIS measurement to ensure the complete formation of $Li_4Ti_5O_{12}$ electrode. It is interesting to note that the EIS of $Li_4Ti_5O_{12}$ without and with 3 wt% carbon addition are composed of one depressed semicircle at high to middle frequency and a slope line at low frequency, while the EIS of $Li_4Ti_5O_{12}$ with 5 wt% carbon addition are composed of two partially overlapped and depressed semicircles at high to middle frequency and a slope line at low frequency [33-36].

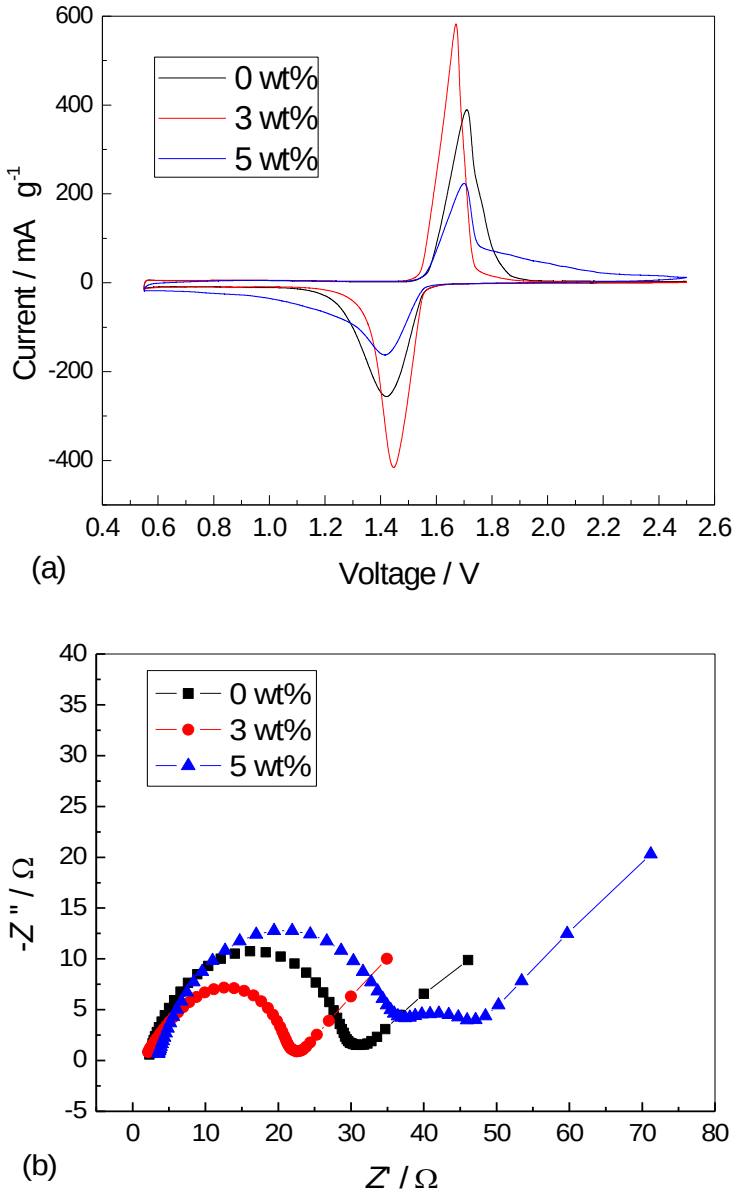

Figure 5. CV (a) and EIS (b) of $Li_4Ti_5O_{12}$/C composite with 0, 3 and 5 wt% carbon additions.

From Table 1, the BET surface area of $Li_4Ti_5O_{12}$ sample with 5 wt% carbon addition is much larger than those of other samples. This much higher content of free amorphous carbon may contribute to the secondary depressed semicircle of EIS. The intersection of the slope line with real axis refers to a bulk resistance (R_b), which reflects the electronic and ionic resistance of two electrodes and electrolyte/separator. Obviously the sample with 5 wt% carbon addition has a larger R_b than other samples. The $Li_4Ti_5O_{12}$ electrodes were charged and discharged three times between 1.0 V and 2.5 V (vs. Li/Li^+) before EIS test. Thus, there is no SEI formation on the $Li_4Ti_5O_{12}$ material surface during the charge and discharge process, since the reaction of SEI formation occurs below 0.8 V (vs. Li/Li^+) [37-38]. The primary depressed semicircle at high to middle frequency for the $Li_4Ti_5O_{12}$ without and with 3wt% carbon addition can be attributed to the charge-transfer resistance (R_{ct}) and CPE1, and the secondary depressed semicircle at medium frequency range as that of $Li_4Ti_5O_{12}$ with 5 wt% carbon

addition can be attributed to the resistance of surface redox Faradaic reactions and CPE2. CPE1 and CPE2 are the constant phase elements used in places of double-layer capacitance and redox capacitance, respectively. The slope line at low frequency corresponds to the Warburg impedance (Z_w), which is related to the Li-ion diffusion in the electrodes [35]. Fig. 5b also shows that the R_{ct} of $Li_4Ti_5O_{12}$ with 3wt% carbon addition is the least and that with 5 wt% carbon addition the largest. The larger R_{ct} is mainly attributed to the agglomeration of carbon resulting in a great decrease of ionic conductivity. It is seen that the EIS results are consistent with those of the CV.

3.7 Rate-discharge performance of $Li_4Ti_5O_{12}$/C composite

Figure 6 shows the rate-discharge performance of $Li_4Ti_5O_{12}$/C composite. The specific capacities of $Li_4Ti_5O_{12}$ with 0, 3 and 5 wt% carbon addition at 0.1 C (the current density of 1 C is 175mAg^{-1}) are 159.9, 165.6 and 162.4 mAhg^{-1}, respectively, which are very close to the theoretical capacity of $Li_4Ti_5O_{12}$ (175 mAhg^{-1}). For the $Li_4Ti_5O_{12}$ sample without carbon addition, the capacities with discharge rates of 1, 3 and 5 C are 145.3, 121.2 and 106.0 mAhg^{-1}, respectively. The capacities of 1, 3 and 5 C discharges of the $Li_4Ti_5O_{12}$ sample with 3 wt% carbon addition are respectively 151.4, 132.1 and 117.5 mAhg^{-1}, which are slightly larger than the correspondent results of 147.4, 127.9 and 114.9 mAhg^{-1} of the $Li_4Ti_5O_{12}$ sample with 5 wt% carbon addition. It is seen that the carbon addition can improve the specific capacity and rate discharge performance of $Li_4Ti_5O_{12}$ samples. However, excessive carbon addition, as of the case of 5 wt%, results in a slight decrease in the specific and rate discharge capacity and the discharge potential. This decrease is attributed to the larger polarization resulted from the much agglomeration of carbon. In a word, the $Li_4Ti_5O_{12}$/C samples synthesized by the solid-state method using amorphous TiO_2 nanoparticles exhibit high specific capacity and good rate discharge performance. The $Li_4Ti_5O_{12}$/C samples show much more excellent rate discharge and voltage plateau properties than previous reports using amorphous TiO_2 [30-31].

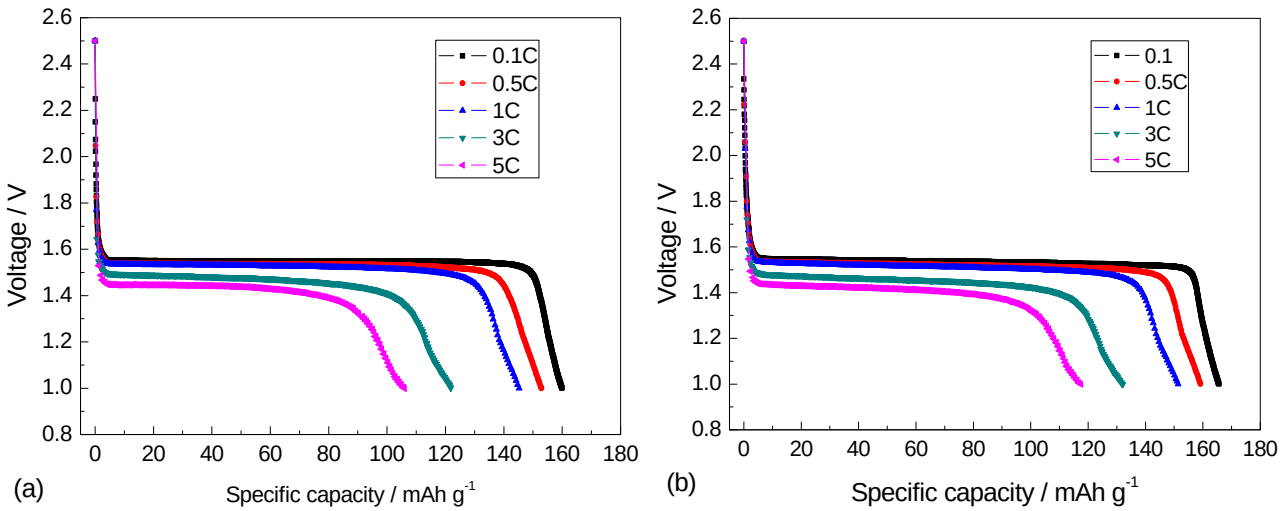

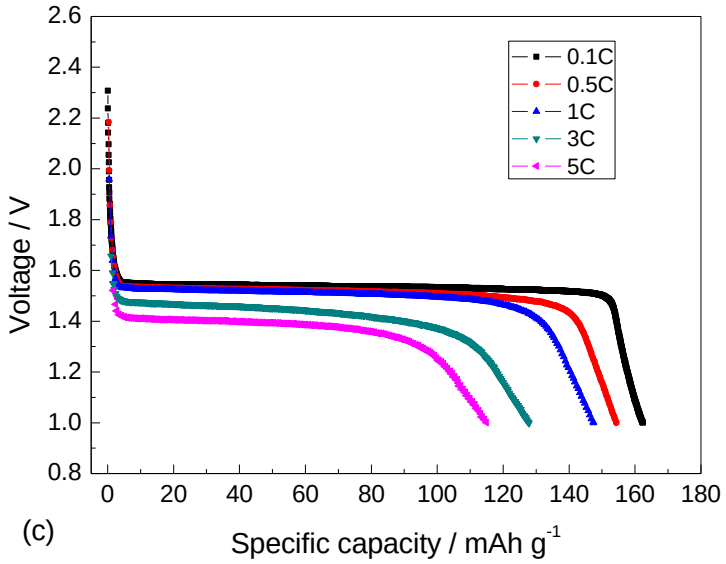

Figure 6. Rate-discharge of $Li_4Ti_5O_{12}$/C composite with different carbon additions: (a) 0 wt%, (b) 3 wt%, and (c) 5 wt%.

3.8 Cycling performance of $Li_4Ti_5O_{12}$/C composite

Fig. 7 presents the cycling performance of nano-$Li_4Ti_5O_{12}$/C composite at 1 and 5 C. It is interesting to not that the $Li_4Ti_5O_{12}$/C composite with 5 wt % carbon addition shows much better cycling performance than that of samples of 0 and 3 wt % carbon addition. The capacity retention of samples with 0, 3 and 5 wt % carbon addition after 600 cycles at 1 C is 83.72, 81.54 and 99.86%, respectively, and that after 600 cycles at 5 C is respective 78.90, 81.70 and 92.95%.

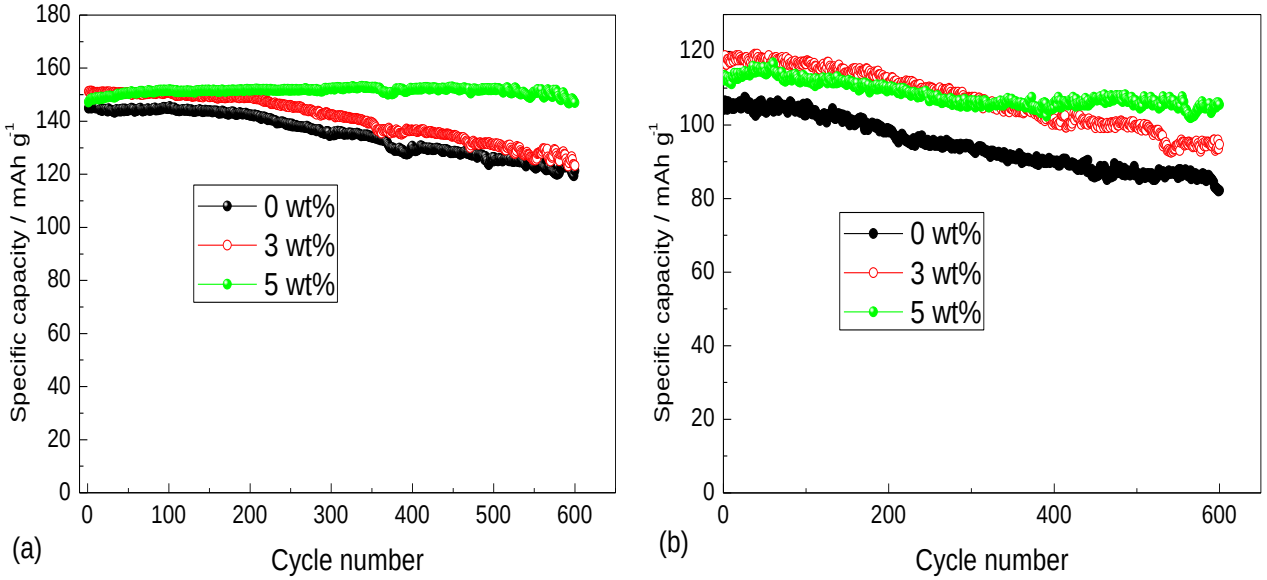

Figure 7. Cycle performance of $Li_4Ti_5O_{12}$/C composite with different discharge rate: (a) 1C and (b) 5C.

This result seems contradictory with the results of CV and EIS. Whereas, from CV of Fig. 5a, we obtain that the charge storage mechanism the sample with 5 wt% carbon addition may include the lithium ion lithiation and capacitive behavior. The larger polarization is attributed to the much agglomeration of carbon, and does not due to the bad reversibility $Li_4Ti_5O_{12}$ crystal. Thus, it can be obtained that the capacitive behavior of the sample with 5 wt% carbon addition is beneficial for the improvement of its cycling performance.

3. CONCLUSIONS

The amorphous TiO_2 nanoparticles were prepared by microemulsion method, and then were used to synthesize the $Li_4Ti_5O_{12}$/C composite. It is found that the $Li_4Ti_5O_{12}$/C composites with excellent electrochemical performance can be synthesized under lower temperature and shorter time and their grain size is less than 400 nm. The carbon addition plays a significant influence of structure, morphology, and electrochemical performance of composite. The sample with 3 wt% carbon addition almost does not contain free amorphous carbon and impurity phases, and shows highest specific capacity and they are 165.6, 151.4 and 117.5 $mAhg^{-1}$ at 0.1, 1 and 5 C rate, respectively. Whereas, the sample with 5 wt% carbon addition shows best cycling performance and the capacity retention after 600 cycles at 1 and 5 C is respective 99.86% and 92.95%. Its capacitive behavior is beneficial for the improvement of the cycling performance.

ACKNOWLEDGEMENTS
This work was supported by China Postdoctoral Science Foundation (No. 20100470296), National Nature Science Foundation of China (No. 50802049 & No. 50632040) and Shenzhen Technical Plan Project (NO. JP200806230010A & No. SG200810150054A), Guangdong Province Innovation R&D Team Plan for Energy and Environmental Materials.

References

1. E. Ferg, R. J. Gummow, A. d. Kock, M. M. Thackeray, *J. Electrochem. Soc.*, 141 (1994) L147.
2. T. Ohzuku, A. Ueda, N. Yamamoto, *J. Electrochem. Soc.*, 142 (1995) 1431.
3. L. Aldon, P. Kubiak, M. Womes, J. C. Jumas, J. Olivier-Fourcade, J. L. Tirado, J.I.Corredor, C. P. Vicente, *Chem. Mater.*, 16 (2004) 5721.
4. S. S. Zhang, K. Xu, T. R. Jow, *Electrochim. Acta*, 51 (2006) 1636.
5. H. Schranzhofer, J. Bugajski, H. J. Santner, C. Korepp, K.-C. M¨oller, J. O. Besenhard, M. Winter, W. Sitte, *J. Power Sources*, 153 (2006) 391.
6. S. S. Zhang, K. Xu, T. R. Jow, *J. Power Sources*, 130 (2004) 281.
7. T. Doi, Y. Iriyama, T. Abe, Z. Ogumi, *Chem. Mater.*, 17 (2005) 1580.
8. A.Guerfi, S. Sevigny, M. Lagace, P. Hovington, K. Kinoshita, K. Zaghib, *J. Power Sources*, 119 (2003) 88.
9. L. Cheng, H.-J. Liu, J.-J. Zhang, H.-M. Xiong, Y.-Y. Xia, *J. Electrochem. Soc.*, 153 (2006) A1472.
10. Y. Abe, E. Matsui, M. Senna, *J. Phys. Chem. Solids*, 68 (2007) 681.
11. T. F. Yi, J. Shu, Y. R. Zhu, X. D. Zhu, R. S. Zhu, A. N. Zhou, *J. Power Sources*, 195 (2010) 285.

12. D. Capsoni, M. Bini, V. Massarotti, P. Mustarelli, G. Chiodelli, C. B. Azzoni, M. C. Mozzati, L. Linati, S. Ferrari, *Chem. Mater.*, 20 (2008) 4291.
13. J. Wolfenstine, J. L. Allen, *J. Power Sources*, 180 (2008) 582.
14. S. H. Huang, Z. Y. Wen, X. J. Zhu, Z. H. Gu, *Electrochem. Commun.*, 6 (2004) 1093.
15. S. Huang, Z. Wen, B. Lin, J. Han, X. Xu, *J. Alloys Compd.*, 457 (2008) 400.
16. S. Ji, J. Zhang, W. Wang, Y. Huang, Z. Feng, Z. Zhang, Z. Tang, *Mater. Chem. Phys.*, 123 (2010) 510.
17. J. Wang, X.-M. Liu, H. Yang, X.-d. Shen, *J. Alloys Compd.*, 509 (2011) 712.
18. G. J. Wang, J. Gao, L. J. Fu, N. H. Zhao, Y. P. Wu, T. Takamura, *J. Power Sources*, 174 (2007) 1109.
19. J. J. Huang, Z. Y. Jiang, *Electrochim. Acta*, 53 (2008) 7756.
20. X. Li, M. Z. Qu, Y. J. Huai, Z. L. Yu, *Electrochim. Acta*, 55 (2010) 2978.
21. X. Li, M. Z. Qu, Z. L. Yu, *Solid State Ionics*, 181 (2010) 635.
22. T. Yuan, X. Yu, R. Cai, Y. K. Zhou, Z. P. Shao, *J. Power Sources*, 195 (2010) 4997.
23. M. Venkateswarlu, C. H. Chen, J. S. Do, C. W. Lin, T. C. Chou, B. J. Hwang, *J. Power Sources*, 146 (2005) 204.
24. Y. H. Rho, K. Kanamura, *J. Electrochem. Soc.*, 151 (2004) A106.
25. T. Yuan, K. Wang, R. Cai, R. Ran, Z. P. Shao, *J. Alloys Compd.*, 477 (2009) 665.
26. J. Shu, *J. Solid State Electrochem.*, 13 (2009) 1535.
27. L. X. Yang, L. J. Gao, *J. Alloys Compd.*, 485 (2009) 93.
28. J. Li, Y. L. Jin, X. G. Zhang, H. Yang, *Solid State Ionics*, 178 (2007) 1590.
29. T. Yuan, R. Cai, R. Ran, Y. K. Zhou, Z. P. Shao, *J. Alloys Compd.*, 505 (2010) 367.
30. J.-w. YANG, H. ZHONG, H.-y. ZHONG, Y.-y. DAI, X. ZHAO, *The Chinese Journal of Process Engineering*, 5 (2005) 170.
31. X.-y. WANG, Y.-s. WANG, X.-y. WANG, L.-l. JANG, W.-m. LONG, Q.-q. CHEN, L. LIU, *Natural Science Journal of Xiangtan University*, 32 (2010) 57.
32. J. Gao, J. R. Ying, C. Y. Jiang, C. R. Wan, *J. Power Sources*, 166 (2007) 255.
33. F. Nobili, R. Tossici, F. Croce, B. Scrosati, R. Marassi, *J. Power Sources*, 94 (2001) 238.
34. F. Croce, F. Nobili, A. Deptula, W. Lada, R. Tossici, A. D'Epifanio, B. Scrosati, R. Marassi, *Electrochem. Commun.*, 1 (1999) 605.
35. M. Umeda, K. Dokko, Y. Fujita, M. Mohamedi, I. Uchida, J. R. Selman, *Electrochim. Acta*, 47 (2001) 885.
36. G. T. K. Fey, W. H. Yo, Y. C. Chang, *J. Power Sources*, 105 (2002) 82.
37. Y.-B. He, Z.-Y. Tang, Q.-S. Song, H. Xie, Y.-G. Liu, Q. Xu, *J. Electrochem. Soc.*, 155 (2008) A481.
38. C. Wang, A. J. Appleby, F. E. Little, *Electrochim. Acta*, 46 (2001) 1793.